Endocrine, *vol. 17, no. 1, 5–14, February 2002* 0969–711X/02/17:5–14/$12.50

Morphologic Detail of Aging Bone in Human Vertebrae

Alan Boyde

Department of Anatomy and Developmental Biology, University College London, UK

To investigate aging bone structure of humans—here, in the lumbar vertebral bodies—requires methodologies that have sufficiently high resolving power yet still have sufficient width and depth of field. No clinical imaging method can come close to meeting the first requirement, leading to the disadvantage of being limited to postmortem studies. Few microscopic methods meet the second and third requisites. The three-dimensional (3D) images of bone in this article were obtained using deep-field 3D optical imaging, X-ray imaging, and scanning electron microscopy (SEM) of macerated plane parallel slices. The study of bone as a 3D object provides a different perspective from conventional two-dimensional images, and enriches our understanding of how modeling and remodeling processes regulate bone structure and connectivity. The study of ultraflat block surfaces by quantitative backscattered electron imaging permits acquisition of data on mineral distributions and densities within a very thin layer (a continuous and perfect very thin section) in the block face. With this information, bone can be viewed as a spectrum of tissue types varying in degree of mineralization.

Key Words: Osteoporosis; bone turnover; bone density; mineralization; aging.

Introduction

A common view of bone remodeling accepts that bone is removed within a given area by osteoclasts and, after an interval, replaced in the same domain by osteoblastic activity. In modeling, the resorption and formation of bone may occur at different locations, enabling changes in the shape and drift of bone in space. In both remodeling and modeling, a net loss of bone mass results if the total amount of bone replaced is less than that removed. Conventional thought is that changes in cancellous bone architecture result as a consequence of thinning and perforation of trabecular plates owing to resorption occurring on both sides of a platelike structure. Once trabecular bone has been perforated, current dogma holds that it cannot be reconstructed because the local template is missing. This basic scheme only partially explains the changes seen in aging and osteoporosis. Refined approaches to imaging bone lead to additional insights on its structure and turnover.

Author to whom all correspondence and reprint requests should be addressed: A. Boyde, Department of Anatomy and Developmental Biology, University College London, Gower Street, London, WC1E 6BT, UK. E-mail: a.boyde@ucl.ac.uk

How to Image Bone Microstructure?

Much of our knowledge of human bone histomorphometry literature is based on two-dimensional (2D) images of cancellous bone of the iliac crest, since this site is considered safe and acceptable for the surgery needed to biopsy a small cylinder of bone. Although light microscopic histomorphometric determination of bone volume fraction from histology sections can give helpful results for diagnosis of disease, the tissue volume sampled by such procedures is unrepresentative of the skeleton at large, especially of weight-bearing bones.

The interconnectedness of trabeculae can only be appreciated in intact tissue; this is unavoidably lost when bone is rendered into the typically 10-µm-thick sections used for light microscopy. The iliac crest site usually has a highly anisotropic architecture, which means that the degree of apparent connectivity depends on the rotation of the plane of section with respect to the long axis of the cylindrical biopsy. Studies of 2D sections may report on the numbers of free ends in the trabecular structure. While it is true that some trabeculae may be cut through by osteoclastic resorption, studies of autopsy material (where more of a bone can be sampled) using 3D imaging technologies show that every single apparently isolated morsel of bone at the surface of a section is, in reality, connected to other bone.

Complete three-dimensional (3D) reconstructions for studying the integrity of tissue organization can be generated either by cutting as many physical sections as are needed to encompass the entire bone *(1)* or via reconstructions based on high-resolution (micro) computed tomography (CT) *(2)*. These methods require significant capital investment and have limitations in resolution: the resolving power of µCT is not as good as what is easily obtained in light microscopy. In the best clinical circumstances, namely peripheral quantitative of the distal forearm, the resolution barely exceeds that possible with the naked eye. It is not yet possible to resolve correctly the fine structure boundaries between trabecular bone and marrow, cortical bone and periosteum, and trabecular-cortical connections. In a common example

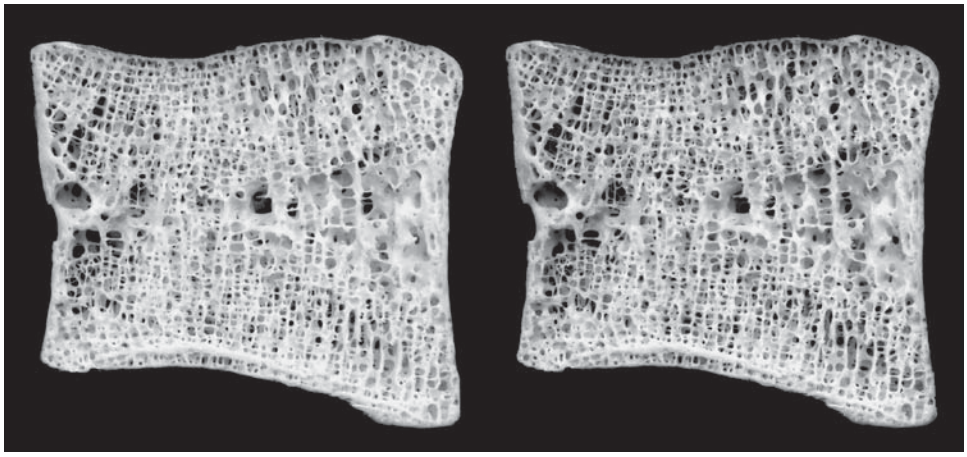

Fig. 1. Stereo pair image of L4 from 30-yr-old female. The unembedded parasagittal 2.8-mm-thick was slice cleaned using bacterial enzyme detergent, dried, and imaged with a UMAX UTC-5400 flatbed scanner using 60-mm shift to generate the stereo parallax. The anterior surface is shown on the left with the double plate on the inferior surface below. Line-of-sight pore spaces appear black.

of a mistaken assumption, conventional radiography and CT imaging appear to show that the human lumbar vertebral bodies have substantial cortices. The naked eye study of macerated bone samples shows that the cortical bone of the vertebral body is normally a shell scarcely thicker than the trabeculae (Fig. 1).

Methods

We need to be more aware of the limitations of the conventional light microscopy bone histomorphometry database from which many of the concepts of bone remodeling phenomena have been derived. I next make a few comments about the techniques that I favor and mention some of the principal insights that they have provided.

Simplest, Deep-Field Optical Methods

Direct inspection and optical imaging of cleaned slices remains a very cheap and effective method to study bone architecture and porosity. 3D imaging for offline viewing by remote third parties can be achieved with stereophotography *(3,4)* or by video image display of continuously rotating beam or rod-shaped samples *(5)*.

A slice <2 mm thick can be scanned directly in a 35-mm slide scanner. The thickness limitation does not apply if flatbed (document) scanners are used. The modern flatbed scanners have really marvelous resolution (with pixel sizes of 10 μm) and outstanding depth of field. This makes them ideal in generating in-depth images of trabecular bone slices. Even more remarkable are the stereo images that can be constructed by this technology (Figs. 1 and 2) *(6)*. However, the proper interpretation of bone surface activities in unembedded cancellous bone samples requires 1-μm resolution with substantial width and depth of field, and this combination cannot be achieved by such simple optical methods. Neither can current confocal light microscopy tackle this job, which belongs to scanning electron microscopy (SEM).

Digital Analysis of Radiographic Images of Plane-Parallel Slices of Trabecular Bone

Digital image analysis of high-resolution X-ray images of plane-parallel slices can be used to demonstrate variations in average local bone mass. Figure 3 shows the extent to which net radiodensity may vary within small defined regions of a human lumbar vertebra. Even with substantial global averaging within the bone slice, it can be seen that regional bone mineral density or volume fraction in large subvolumes of roughly 48 mm^3 (4 × 4 mm in area × 3 mm in depth) may vary by a factor of 4:1.

Advances in 3D SEM Using Fast Electrons

SEM today covers the entire range of fields of view across a bone slice needed for studies at higher resolutions and remains the technology of choice for studies of the fine structure of bone *(7,8)* (Figs. 4–7).

In SEM, we recognize the type of bone surface activity from morphology. *Resting* surfaces show complete, intact, collagen fiber bundles in anorganic or deproteinized samples in which all marrow, cells, and nonmineralized matrix has been removed. The relative age of a superficial bone packet can be judged from the strength of electron backscattering, older and therefore more mineralized matrix giving a stronger signal, other geometric factors being equal (not illustrated here). *Forming* surfaces have mineralizing fronts and are recognized by the broken-up pattern of the matrix collagen. *Resorbed* surfaces are easily spotted by the characteristic morphology of the osteoclastic resorption pits or excavations: these vary from being deep and round, to shallow and more elongated where the osteoclast migrated during or between episodes of its resorptive activity (Figs. 4–7).

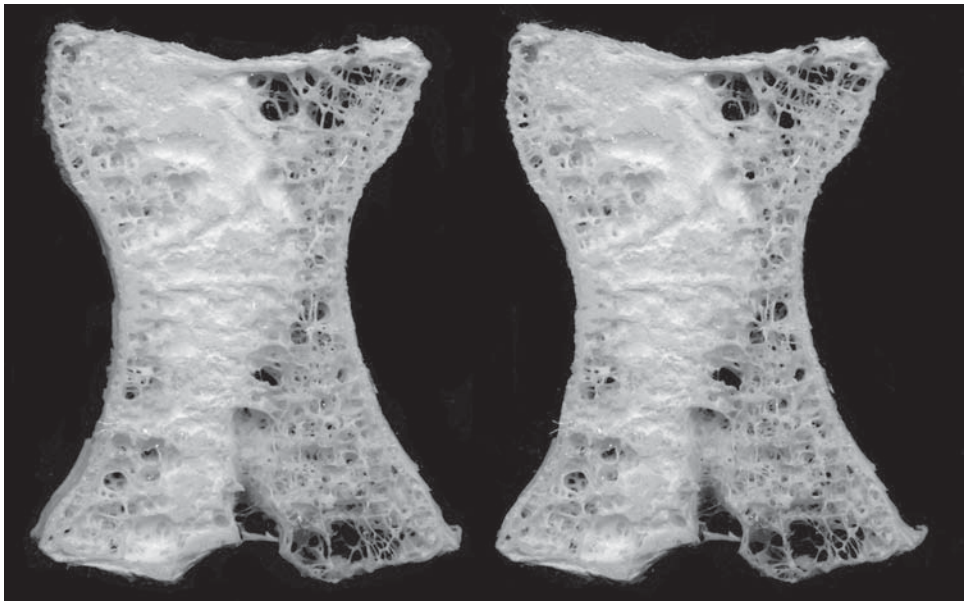

Fig. 2. Stereo pair image of L3 lumbar vertebral body from 71-yr-old female. The cleaned, dried, unembedded parasagittal 3-mm slice was imaged using 45-mm shift with a UMAX UTC 5400 flatbed scanner. The anterior surface is shown at the top and the superior surface on the left. Note central compression and reduction in line-of-sight porosity.

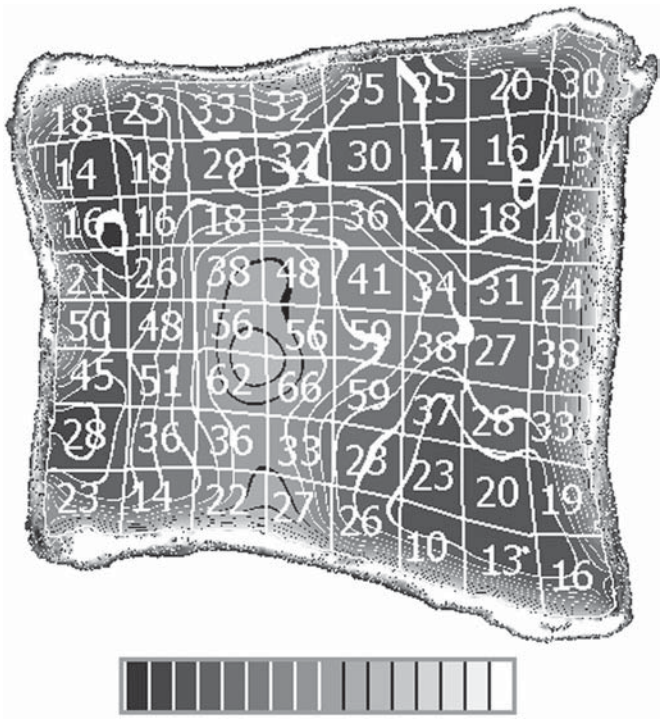

Fig. 3. Heavily smoothed digitized radiographic image of unembedded, cleaned 3-mm parallel slice of L4 from an 89-yr-old female. The anterior surface is shown on the left. Range extends from 0% (black, no bone present) to 100% (solid bone). Numbers in white are mean percentage of bone in total volumes of approx 3 × 3 × 4 × 4 mm. Note the extreme range shown in different regions, with the highest bone volume recorded in the central superior-inferior third. Gray level contours follow regions with equal X-ray absorption.

A great advantage of SEM over light microscopy is the ability to survey the bone surface activity state efficiently and extensively. Looking at both sides of the sample when studying thick slices (2 mm slices of normal or 4-mm slices of porotic) of vertebral trabecular bone, inspection can cover >80% of surfaces in the clearest 3D context. This is in sharp contrast with the miniscule fractions of total tissue surface examined by routine bone histomorphometry.

Most biologic SEM to date has employed mainly the slow or secondary electrons leaving the sample surface under electron bombardment (Fig. 7). Like other biologic materials, bone—dry because it is in a vacuum—is not electrically conductive. Technical problems arise because of local charging of declivities in the sample surface that cannot be reached with surface-coating procedures (SEM samples are most often coated with metals such as gold; I use carbon). These charging problems depart if we only employ fast-scattered electrons, which also give the benefit of traveling in straight paths to a suitable detector.

One aim of my recent work has been to enhance information content in SEM images by using separate recordings from multiple backscattered electron (BSE) detectors. In a typical example, each image field is documented with at least four scans with as many separate detectors. Data can then be interpolated to emulate acceptance angles into 8, 16, 32, or more virtual detectors. On a computer screen, or using a data projector, playing resultant images in sequence continuously sweeps the apparent direction of illumination and powerfully increases depth interpretation through motion

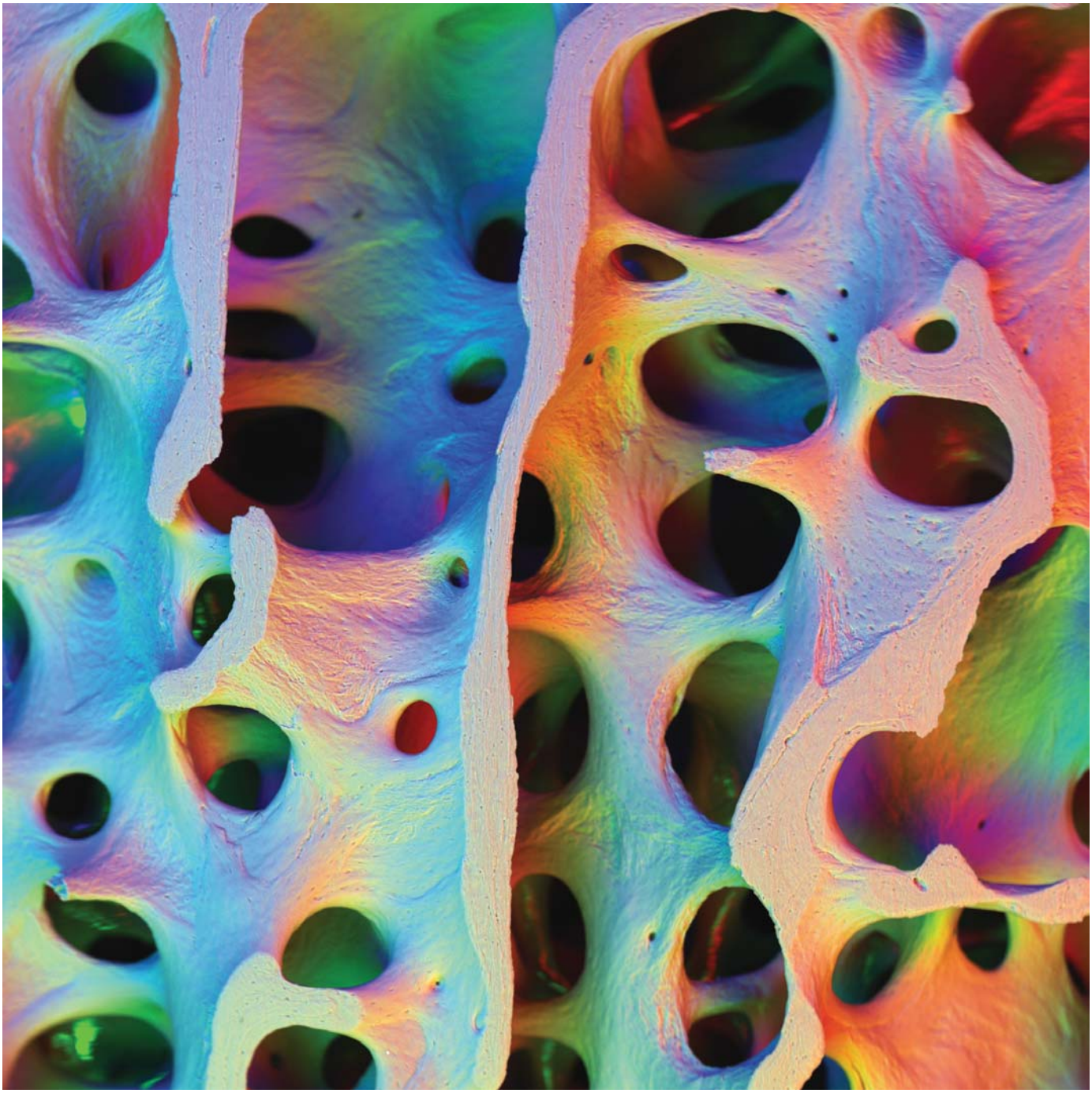

Fig. 4. BSE SEM image of parasagittal slice of trabecular bone from L4 of a 31-yr-old male. Information from three of four BSE detectors is coded as red, green, or blue components to create composite color images. Field: 4.45 mm wide × 4.45 mm high, 4-mm-thick sample.

parallax. In addition, the sample may be moved continuously such that image sequence replay emulates linear motion parallax from flying past the surface.

Further enhancement of 3D understanding can be achieved through spectral color coding of the direction of illumination, which allows wider sectors of total data sets to be exploited simultaneously (Figs. 4 and 5).

Another recent advance in SEM imaging concerns processing stacks of through-focus series, acquired by mechanical stage stepping, to select information representing the best focus within each area in a composite output representation (unpublished data) (Fig. 6).

Composition: Quantitative BSE Imaging

Over time, mineral replaces water in bone matrix, and the increasing mineral content progressively increases bone stiffness. This, together with the collagen weave, is also an important parameter in determining the local mechanical

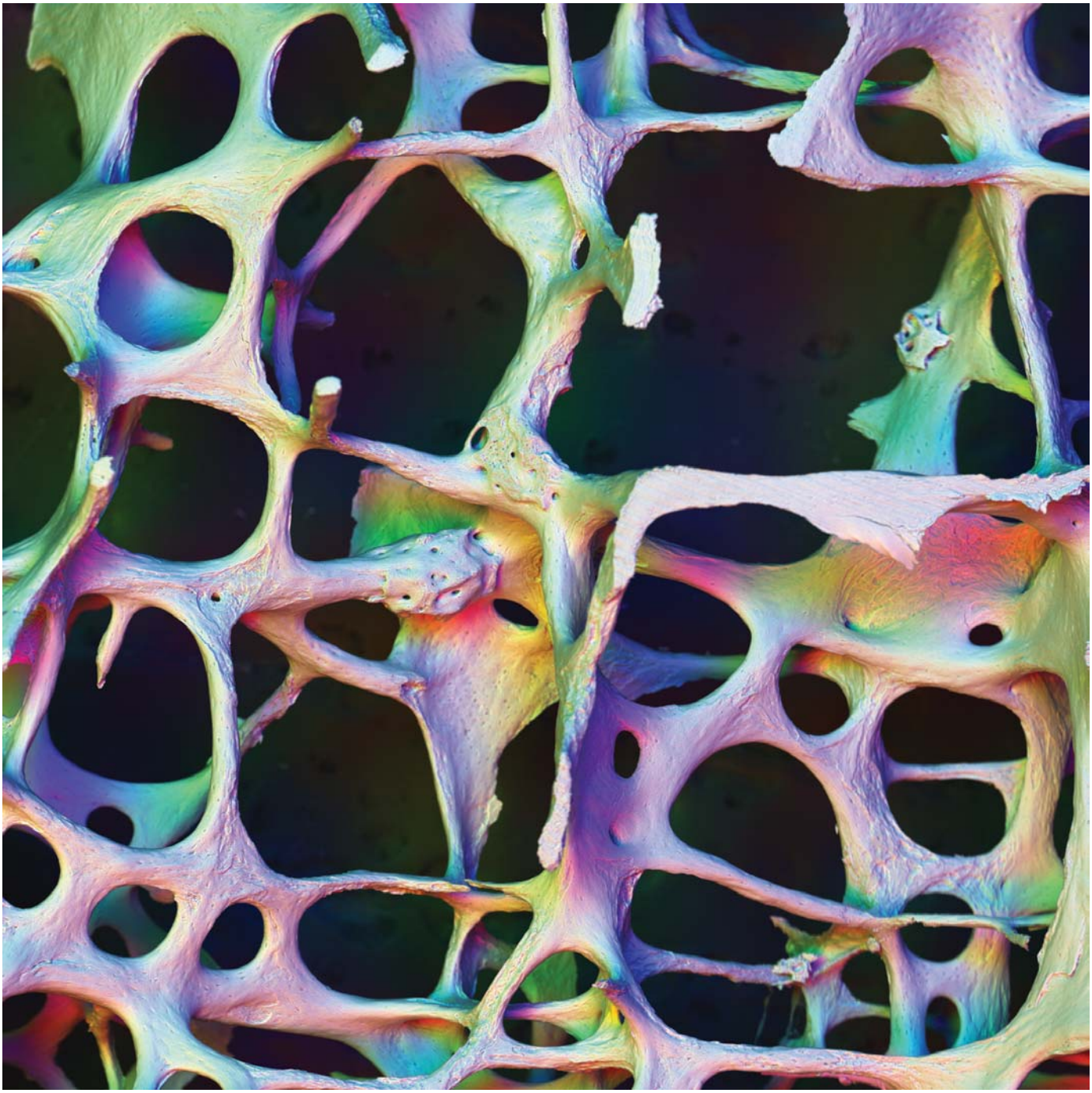

Fig. 5. BSE SEM image of parasagittal slice of trabecular bone from L4 of 89-yr-old female. Information from three of four BSE detectors is coded as red, green, or blue components to create composite color images. Field: 4.689 mm wide × 4.689 mm high, 2.8-mm-thick sample.

properties of the tissue. Since the earliest days of microradiography, it has been known that the bone mineral content in a microscopic volume of bone generally increases with the age of the bone tissue element. Newly deposited bone packets are less well mineralized. That there has to be an optimum level of mineralization can be seen by the study of diseases in which this is not achieved (see Fig. 8, E,F).

We study bone mineralization at the microscopic scale using quantitative BSE (qBSE) (Fig. 8). To perform qBSE studies, it is necessary to fill marrow and cell space with a material of uniform composition that is both vacuum and electron beam stable. The specimen may not have surface topographic features if one is to exploit the composition dependency of the BSE signal. To accomplish this, methylmethacrylate monomer is polymerized *in situ* after having first removed water and fat with ethanol. Micromilling (Reichert-Jung UltraMiller, Leica, UK) is used to finish the polymethyl methacrylate (PMMA) blocks, and the aim is to

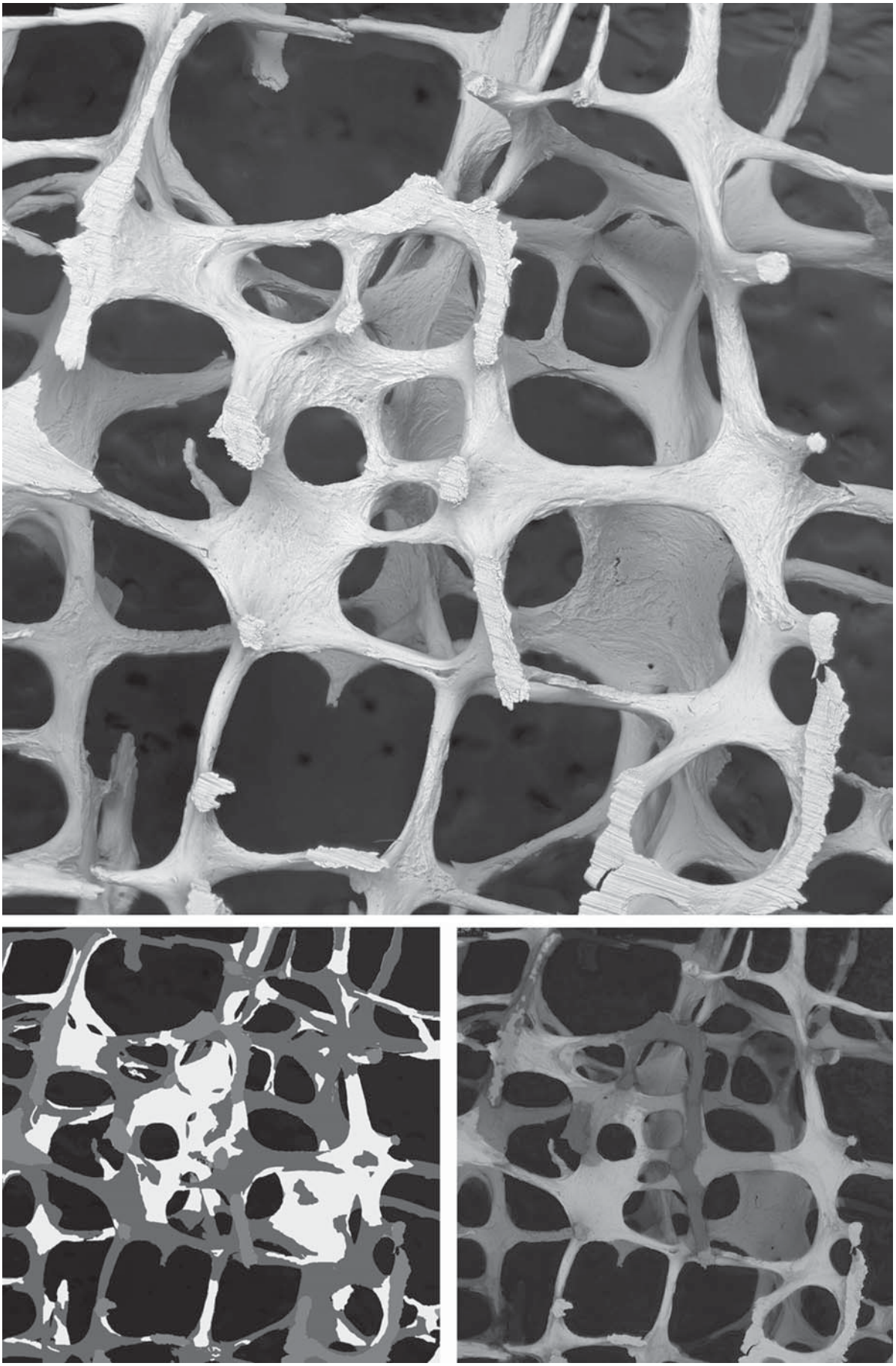

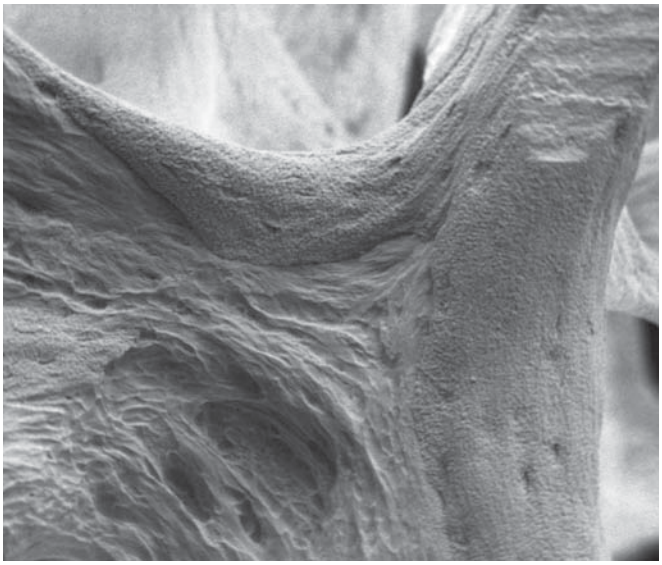

Fig. 7. Parasagittal section of L4 from a 75-yr-old female, cleaned with bacterial enzyme detergent and hydrogen peroxide to remove all cells and osteoid. Two parts of same bone packet converge (**center**) at junction of rod (**top right**) with plate (**lower left**). New bone was forming over intact and therefore fully mineralized collagen bundles, although this is close to resorbed surfaces in the lower part of the field. Field width: 470 μm. A secondary electron image of gold sputter–coated sample is shown.

produce surfaces that are flat to within 0.1 μm. By using a very stable digital automated scanning electron microscope (Zeiss DSM962 with Kontron IBAS external control computer and an annular solid-state BSE detector), signal brightness from one spot to another can be compared. Signal brightness will depend principally on variations in composition of the tissue, and in particular on its mineral content. In my laboratory, we standardize our observations by referring BSE signal values to those obtained from suitable standard compounds. To avoid electron channeling contrast, the standard sample must have no long-range crystallographic order. For this purpose, we use brominated and iodinated dimethacrylate resins *(16,17)*. We arbitrarily divide bone into a number of subclasses depending on the standardized, measured qBSE value, using the same colors to show bone in equivalent portions of the spectrum of possible mineralization densities (Fig. 8). We make very large numbers of repeat measurements from very small volumes. At about 1 μm^3, the sampled points are generally within or outside bone tissue proper and are not seriously affected by partial volume effects, a concern in plain radiography, tomography, peripheral CT, and CT.

Fig. 6. Another field from same sample of L4 from 89-yr-old female (field: 4.45 mm wide × 4.45 mm high, 2.8-mm-thick sample. (**A**) Computer processing of information from series of 11 levels at 250 μm mechanical focus difference, each level recorded separately with four BSE detectors to give an image in good focus irrespective of depth, thus allowing better discrimination of bone surface activity; (**B**) cut edges shown as medium gray, resorbed areas as light color, other resting and mineralizing-front surfaces as darker gray, with line of sight pore space darkest color; (**C**) height contour map representation, with contrasting gray levels, not in a logical sequence, for succeeding contour levels.

The Unseen Interior: Collagen Patterning

The methods considered herein do not directly address the layup of the collagen of the bone matrix, although this can often be well inferred from the pattern of the superficial matrix fibers. SEM easily shows the typical branching-bundle pattern of lamellar bone matrix. Most collagen bundles are parallel to the long axes of slender trabecular rods.

The bulk of the hard tissue in human bones is lamellar (layered), mostly secondary osteonal in nature in compact cortical bone, with extensive regions of circumferential lamellae in periosteal surfaces. The microstructure of lamellar bone is, however, not uniform. Older views presumed that osteonal lamellae demonstrated a criss-cross, plywood structure, with the collagen bundles in alternating lamellae having contrasting orientations. Quantitative circularly polarized light microscopy studies (not illustrated here) of plane-parallel sections of long bones show regions subjected to predominantly tensile loads having a strongly preferred collagen orientation in the applied loading direction, while regions subjected to compressive loads show collagen deviating more strongly from the loading direction *(9,10)*. Thus, outwardly similar areas may differ on the basis of collagen fiber orientation patterns, while within such areas, neighboring domains often have different levels of mineralization *(9–13)*.

Results

Even low-magnification images of thick sections of lumbar vertebrae reveal that the body portion is entirely cancellous, with only a thin cortical shell. In examining 3- or 4-mm-thick vertical slices, few pore spaces give a line of sight through a vertical section from a young mature individual (Figs. 1 and 4). By contrast, a similarly thick slice from the vertebral cancellous bone of an elderly individual appears porous, even though there is still a substantial volume fraction of bone and no sign of collapse or gross morphologic change in the vertebral body (Figs. 5 and 6). This observation reflects the normal age-related *change in the microarchitecture* of the cancellous bone, which may be independent of changes in the bone volume fraction (mass, density, and the related radiodensity). However, after the events following the episode of a vertebral compression (crush) fracture, line-of-sight porosity may be starkly reduced, even if radiodensity is not significantly increased (Fig. 2).

In children, cancellous bone in the vertebral bodies has a foamlike structure, with more bone at the linear junctions

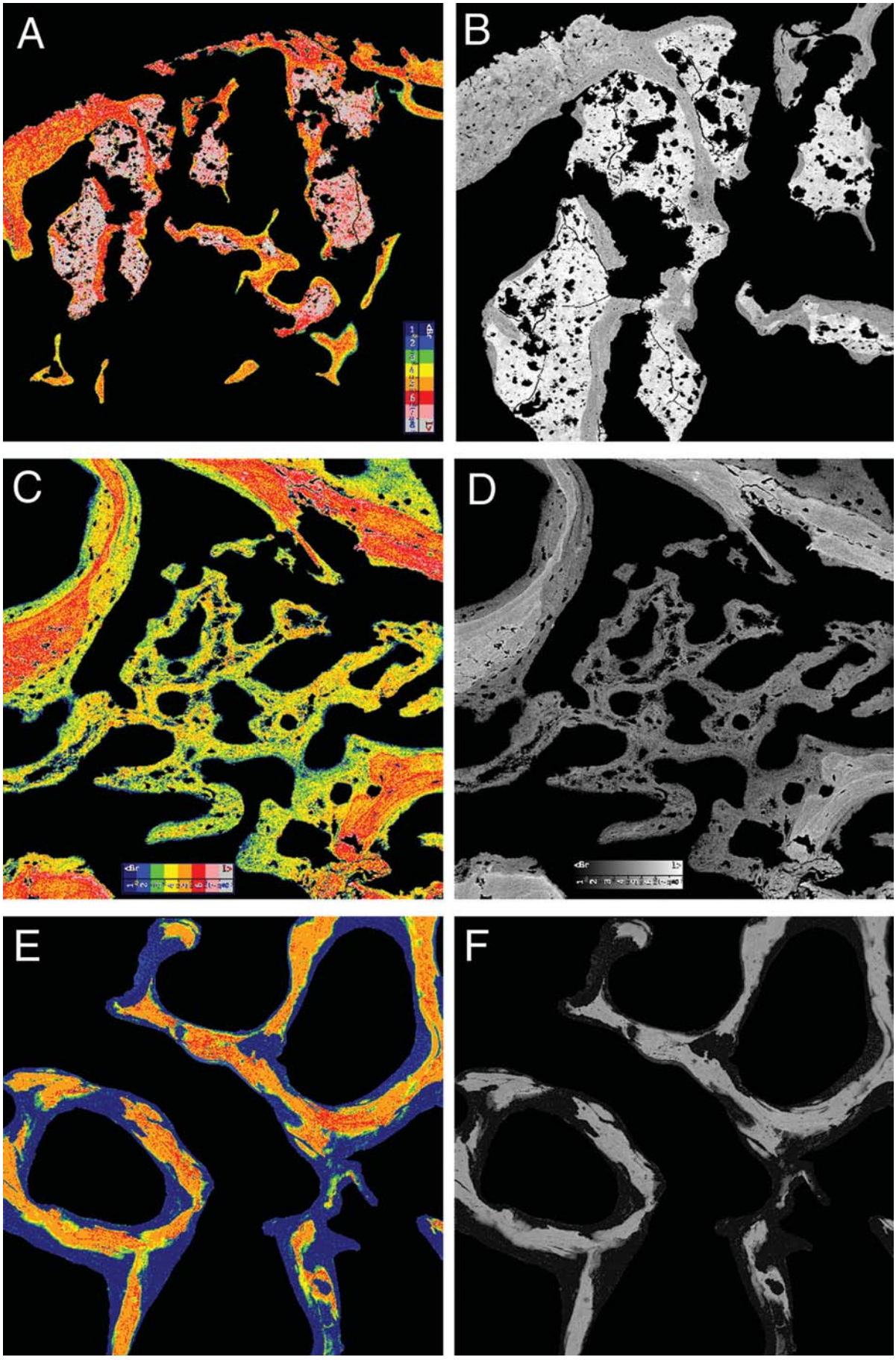
A
B
C
D
E
F

of adjacent marrow chambers apparently forming short rodlike elements, while the bony walls between are perforated *(14)*. In vertical bone sections from children, it may be difficult to recognize the load-bearing direction so easily seen in the adult vertebral body trabecular bone architecture (Figs. 1 and 4). In the younger mature adult, the tissue resembles a vertical honeycomb (but with holes in the walls between chambers) and is evidently porous in thick transverse sections *(3)*. In the older individual, the same platelike cell walls of the honeycomb have been perforated and the structure remodeled and refined to make one of more rodlike elements. In an aging individual, the cancellous bone is a scaffolding of rods. These rods may be quite robust, with the vertical load-bearing elements more so than the horizontal struts. These architectural changes are associated with some loss of bone volume fraction, but there is a proportionately greater increase in the extent of line-of-sight porosity than in bone mass loss.

Increasing gross cortical porosity is a common feature at skeletal sites subject to osteoporotic fracture. In aging humans, there is also a trend toward an increase in the number of defective joins between the old and new bone packets in lumbar vertebral body (Fig. 7). Incompletely mineralized tissue may be incorporated into erstwhile cement lines *(7)*. Resorption with no subsequent repair is often observed. Repair of resorption surfaces may not be site coupled, and repair by microcallus formation can be generalized within bones that exhibit no external signs of collapse (Figs. 5 and 6).

The clear 3D visualization provided by SEM of the surface extent of areas of resorption and of new bone packets shows a generalized deficit in their coupling. Large, unrepaired, resorbed areas become a dominant feature (Figs. 5–7). Vertical load-bearing struts may be fortified with a high proportion of new bone that, from its characteristic fine structure, can be seen to have been added initially as microcallus *(15)*.

Regarding applications of qBSE in imaging normal and pathologic skeletal variations, we have studied large series of human iliac crest biopsy and autopsy samples, second and fourth lumbar vertebral body samples, and femoral neck autopsy samples (unpublished). The unpublished results document the normal range of variation in tissue composition and the normal proportions of volume fractions of bone having compositions different from these skeletal sites. More important, the data show that the level of mineralization in calcified cartilage within bone organs is significantly greater than that of bone tissue proper (Fig. 8 A,B).

In the event of pathologic failure in bone mineralization, such as in rickets and osteomalacia, bones are soft and bend under load. Figure 8 E,F shows the differing distribution of mineral and the lack of it in certain trabeculae in an example of osteomalacia. Perhaps paradoxically at first sight, in the several different types of osteogenesis imperfecta, the tissue reaches a higher level of mineralization than in normal aged-matched bone. The combination of increased mineralization and reduced bone volume fraction contributes to the brittleness characterizing the bones in osteogenesis imperfecta *(16)*.

Conclusion

3D imaging of bone and localized surveys of mineral distribution enhance our understanding of the fine structure of bone and allow us to place the information from conventional bone histomorphometry of more limited samples of bone into context.

Acknowledgments

I am very grateful to Peter Howell and Sheila Jones for their help in many ways, and to Tim Arnett for the loan of the sample shown in Fig. 2. Our facility for quantitative analysis of bone mineralization density at the microscopic scale was established with MRC funding. Micromilling equipment was funded by the Wellcome Trust.

References

1. Odgaard, A. (1998). *Bone* **20,** 315–328.
2. Muller, R., Van-Campenhout, H., Van Damme, B., Van Der Perre, G., Dequeker, J., Hildebrand, T., and Ruegsegger, P. (1998). *Bone* **23,** 59–66.
3. Jayasinghe, J. A. P., Jones, S. J., and Boyde, A. (1994). *Anat. Embryol.* **189,** 259–274.
4. Brickley, M. and Howell, P. G. T. (1999). *J. Archaeol. Sci.* **26,** 151–157.
5. Boyde, A., Radcliffe, R., Watson, T. F., and Jayasinghe, J. A. P. (1990). *Bone* **11,** 228,229.
6. Boyde, A. and Howell, P. G. T. (2002). *Proc. Royal Microsc. Soc.,* in press.
7. Jayasinghe, J. A. P., Jones, S. J., and Boyde, A. (1993). *Virchows. Arch. A Pathol. Anat.* **422,** 25–34.
8. Boyde, A. and Jones, S. J. (1996). *Microsc. Res. Technique* **33,** 93–120.
9. Riggs, C. M., Lanyon, L. E., and Boyde, A. (1993). *Anat. Embryol.* **187,** 231–238.

Fig. 8. qBSE images of PMMA-embedded bone. The color scale insets show the mineralization density scale, with the extremes of the scale established using monobrominated and monoiodinated dimethacrylate standards *(16)*. (**A–D**) Parasagittal slice of L2 from 74-yr-old male. Orientation is anterior (**left**) and superior (**top**). Width and height of the field shown were (A) 5.569 mm and (B) 2.7 mm. The large amount of calcified cartilage (arrow) within the bone domain represents the densest phase present (pink and gray). (**C,D**) L2. Width and height of the field shown were each 0.9 mm. Bone volume fraction is increased by the presence of low-density microcallus, falling in the low-density range represented by yellow, green, and blue on the color scale. (**E,F**) qBSE image of trans-iliac-crest biopsy from a case of nutritional osteomalacia in a 50-yr-old male. Extensive nonmineralized matrix in dark blue band (although commonly called osteoid, this matrix never mineralizes) is shown. Width and height of the field were each 2.7 mm.

10. Riggs, C. M., Vaughan, L. C., Evans, G. P., Lanyon, L. E., and Boyde, A. (1993). *Anat. Embryol.* **187,** 239–248.
11. Portigliatti-Barbos, M., Bianco, P., Ascenzi, A., and Boyde, A. (1984). *Metab. Bone Dis. Rel. Res.* **5,** 309–315.
12. Ascenzi, A. and Boyde, A. (1993). In: *Micromovement in orthopaedics,* Oxford Medical Engineering Series 10. Turner-Smith, A. R. (ed.). Clarendon: Oxford.
13. Goldman, H. M. (2001). PhD Thesis, The City University of New York.
14. Kneissel, M., Boyde, A., Hahn, M., Teschler-Nicola, M., Kalchhauser, G., and Plenk, H. (1994). *Bone* **15,** 539–545.
15. Hahn, M., Vogel, M., Amling, M., Ritzel, H., and Delling, G. (1995). *J. Bone Miner. Res.* **10,** 1410–1416.
16. Boyde, A., Travers, R., Glorieux, F. H., and Jones, S. J. (1999). *Calcif. Tissue Intl.* **64,** 185–190.
17. Boyde, A., Davy, K. W. M., and Jones, S. J. (1995). *Scanning* **17(Suppl. V),** 6,7.